ARTICLE

OBC
www.rsc.org/obc

Cation transport by a redox-active synthetic ion channel

Adam C. Hall,*[a] Cristina Suarez,[b] Anindita Hom-Choudhury,[b] Aida N. A. Manu,[a] C. Dennis Hall,[c] Gregory J. Kirkovits[c] and Ion Ghiriviga[d]

[a] *Department of Biological Sciences, Smith College, MA 01063, USA. E-mail: ahall@smith.edu*
[b] *Department of Chemistry, Smith College, MA 01063, USA*
[c] *Department of Chemistry, King's College, London, UK WC2R 2LS*
[d] *Department of Chemistry, University of Florida, Gainesville, FL 32611, USA*

Received 2nd May 2003, Accepted 23rd June 2003
First published as an Advance Article on the web 10th July 2003

The synthesis, cation binding and transmembrane conductive properties of a novel group of synthetic ion channels containing a redox-active centre are described. Experiments using a black lipid membrane preparation revealed that these compounds function effectively as ion channels. Subsequent ^{23}Na NMR spectroscopy studies focused on a synthesized ion channel with a ferrocene centre. When incorporated in vesicular bilayers, this channel was demonstrated to support a Na^+ flux that was at least six times faster than ion transport by monensin. Since oxidation of the ferrocene moiety completely inhibited the Na^+ transport, the redox-active centre provides a potential mechanism for controlling ion flux.

Introduction

The flux of ions and other materials between extra- and intracellular environments is a fundamental process in all living systems. Small wonder then that extensive research has been devoted to understanding mechanisms of ion transport across cell membranes.[1,2] During the last two decades, efforts have been made to mimic the action of biological ion channels by the synthesis of model systems that span lipid bilayers.[3] Synthetic proteins have been designed[4] to mimic natural channels, albeit with a single span rather than the multiple transmembrane domains typical of biological systems. Other designs include self-assembling cyclic peptide nanotubes that have been shown to destroy bacteria by introducing a pore through the plasma membrane which collapses transmembrane potentials.[5] Recently, artificial channels have been fashioned with head groups (*e.g.* macrocyclic polyethers) to capture specific ions, long aliphatic chains designed to span the bilayer and 'relay units', such as other macrocyclic ethers to shuttle ions across the membrane.[6–10] The 'relay unit' is seen as a potential means of stabilizing cations through hydration by hydrogen-bonded water.[10] This multiple ion transport, known as the 'billiard ball effect' (based on the charge repulsion theory[11]) has been corroborated in channels using other head groups such the calixarenes.[12,13] Electrospray mass spectrometry has served to enhance this view of multiple ion complexation in some artificial channels.[9]

In the following study and a preliminary report,[14] we describe a series of synthetic ion channels containing redox-active centres (both ferrocene and cobaltocenium) represented by $\mathbf{IC_{a–d}}$. (see Fig. 1). Cation binding was studied using ^{13}C-NMR and fluorescence spectroscopy. The latter was dependent on incorporating 9-anthryl units[15,16] into the artificial channels. These fluorophores also served to 'anchor' the channels in the phospholipid bilayer. Finally, we employed cyclic voltammetry to investigate coordination of Na^+ or Ca^{2+} ions with the macrocyclic rings.[14]

We used a variety of techniques to characterize the conductance across bilayers mediated by the novel redox-active ion channels, focusing mainly on $\mathbf{IC_a}$ (see Fig. 1). Ion conduction supported by the other synthesized channels ($\mathbf{IC_{b,c,d}}$) will be addressed in subsequent publications. We assessed cumulative rates of flux promoted by $\mathbf{IC_a}$ and the potential of the ferrocene centre to act as a regulator of ion flux. Biological ion channels

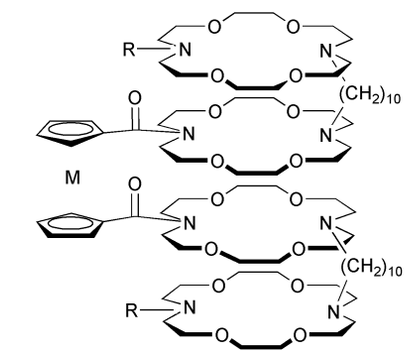

(1)

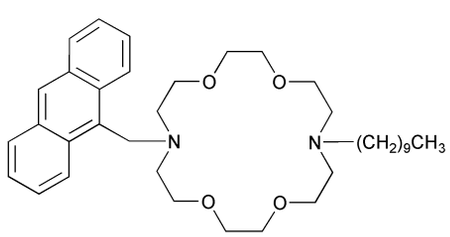

(2)

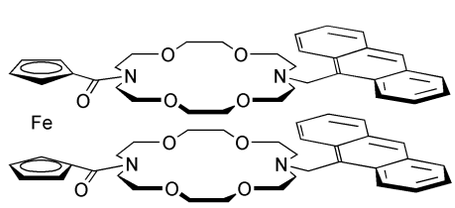

(3)

Fig. 1 (**1**) Structure of the synthetic 1,1′-bis[*N*-carbonyl-*N*′-[10-(*N*′-(9-anthrylmethyl)-diaza-18-crown-6)decyl]-diaza-18-crown-6]ferrocene ($\mathbf{IC_a}$) and analogs. (**2**) and (**3**) containing 9-anthrylmethyl subunits used for the ion channel characterization.

DOI: 10.1039/b304838a

often exhibit the phenomenon of rectification whereby specific ion flux is either favoured or is only permissible at certain membrane potentials. For example, the K^+ inward rectifier channels only allow transport of cations at hyperpolarized (negative) membrane potentials and conductance is switched off during depolarization.[17] Oxaferrocene cryptands have been shown to act as efficient molecular switches for alkaline and alkaline earth metal cations[18] and potentially could perform the same role within a synthetic ion channel. Thus, the incorporation of the ferrocence centre in $\mathbf{IC_a}$ is an attempt to mimic the rectification and switching properties of some natural channels. There are already examples of such redox-mediated synthetic ion channels that include two C-terminus ferrocene derivatives of the natural peptide alamethicin in which ion transport responds to oxidation of the ferrocene.[19]

In preliminary investigations, we used the 'inside-out' patch-clamp technique to record activity induced by introduction of $\mathbf{IC_b}$ to quiescent patches in biological membranes.[14] These experiments (interpreted with caution since $\mathbf{IC_b}$ may have been activating endogenous ion channels) revealed cation transport across membranes with a degree of non-Ohmic behaviour (*i.e.* reduced conductance at positive potentials). To avoid the possibility of activation of endogenous channels, we conducted further experiments using black lipid membrane recordings, thus introducing the synthetic channels to pure lipid bilayers. Recordings of open channel events evoked by $\mathbf{IC_a}$ at different potentials enabled conductance–voltage calculations that were further indicative of weakly rectifying (non-Ohmic) properties.

An alternative and elegant method for characterizing ion channel properties uses pure bilayers in the form of vesicles and ^{23}Na or ^{39}K NMR spectroscopy for measuring the cumulative rates of cation transport across membranes.[20–22] The method relies on monitoring the rate of exchange of the cation between the intra- and extra-vesicular environments where the chemical shift of the 'outside' cation is subject to a chemical shift reagent (*e.g.* Dy^{3+}). This technique has been widely exploited, especially by Gokel *et al.*,[7,8,10] to examine rates of cation transport across membranes infused with artificial channels. In this report, we have adopted the same technique to assess the cumulative rates of cation flux of $\mathbf{IC_a}$ and the impact of oxidation on its ability to behave as a conducting ion channel.

Results and discussion

Synthesis of redox-active ion channels

The ion channel chosen for this particular study ($\mathbf{IC_a}$) is a specific example of the redox-active structures shown in Fig. 1, with R = 9-anthrylmethyl and M = Fe. The synthesis (in overall 7% yield from 1,10-diaza-18-crown-6) was achieved as outlined previously[14] by condensation of mono-*N*-Boc-diaza-18-crown-6 with 9-bromomethyl-anthracene, removal of the protecting group, condensation of the product with 1,10-dibromodecane (1 : 1 molar ratio) condensation of the product with mono-*N*-Boc-diaza-18-crown-6, deprotection of the bicyclic product and condensation of two moles of the resultant amine with 1,1′-ferrocenyl diacid chloride. The compounds were characterized by high resolution mass spectrometry, IR spectroscopy and $^1H/^{13}C$ NMR (see Experimental).

Cation binding by ^{13}C NMR spectroscopy

Complexation of $\mathbf{IC_a}$ with Na^+ (as the trifluoromethyl sulfonate) was first investigated by ^{13}C NMR spectroscopy. Cation binding in the channel induces appreciable changes in the ^{13}C shift values of carbons near the cation. In particular, the chemical shifts of the carbonyl groups, the C-1 and C-4 carbons of the anthryl unit and the anthrylmethylene carbon (Table 1) are most affected and were used as a probe to monitor the binding of Na^+. The results were compared with the C-1 and anthrylmethylene carbons of **2** (see Fig. 1 and Table 2) and

Table 1 ^{13}C shifts [δ_{obs} (ppm)] for selected atoms of ($\mathbf{IC_a}$)

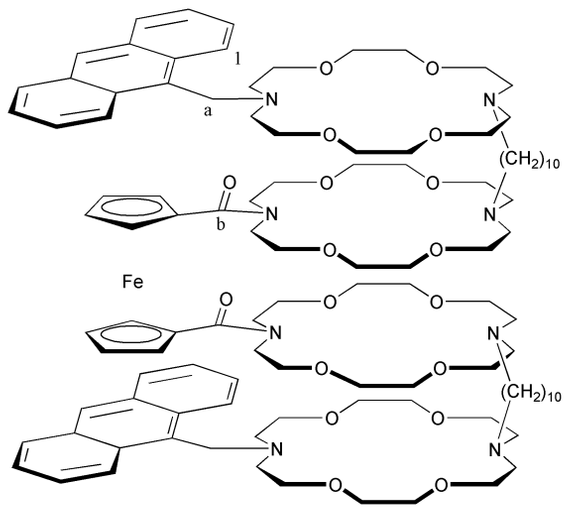

Ratio[a]	C-1	C-a	C-b
0 : 1	126.23	51.82	169.99
1 : 1	[b]	[b]	170.10
2 : 1	126.75	51.02	170.17
3 : 1	127.03	50.69	170.46
4 : 1	127.09	50.60	170.78
10 : 1	127.27	50.52	171.31
$\Delta\delta_{obs}$	+1.04	−1.30	+1.32

[a] Molar ratio $NaSO_3CF_3$ to $\mathbf{IC_a}$. [b] Distinct peak not observed.

Table 2 ^{13}C-shifts [δ_{obs} (ppm)] for selected atoms of (**2**)

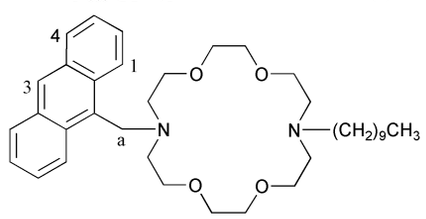

Ratio[a]	C-1	C-4	C-3	C-a
0.00 : 1	126.60	129.76	128.25	52.07
0.25 : 1	126.90	129.90	128.45	[b]
0.50 : 1	127.22	130.07	128.70	51.23
0.75 : 1	127.51	130.23	128.90	50.91
1.00 : 1	127.60	130.28	128.98	50.85
2.00 : 1	127.69	130.33	129.05	50.80
$\Delta\delta_{obs}$	+1.09	+0.57	+0.80	−1.27

[a] Molar ratio $NaSO_3CF_3$ to (**2**). [b] Distinct peak not observed.

clearly there is a parallel between the two sets of data. In the case of **2**, however, a maximum shift was observed at a molar ratio of 1 : 1 indicating complexation of Na^+ within the macrocyclic ring. By contrast, the shifts for $\mathbf{IC_a}$ maximised at about 4 : 1 (Na^+ : $\mathbf{IC_a}$, Fig. 2) indicating multiple coordination within the channel. The shifts suggest that the first two Na^+ions bind with the outer 18-crown-6 units but thereafter, the carbonyl functions and possibly the inner macrocyclic rings become involved in the binding as found earlier in some simpler systems.[23–29] In the case of the ion channel this is indicated by only a slight shift in the carbonyl δ value up to two moles Na^+ but substantial shifts on the addition of 3 or 4 moles of Na^+.

Cation binding by fluorescence spectroscopy

It is well known that fluorescence quenching through photo-electron transfer (PET) from trivalent nitrogen is inhibited by

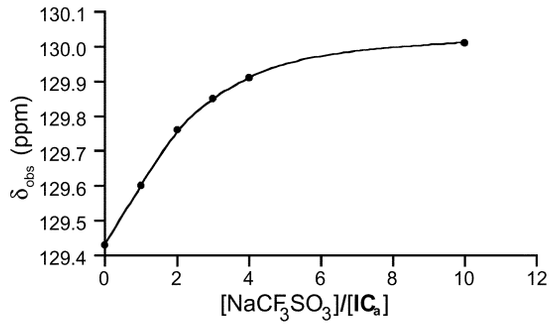

Fig. 2 Plot of ^{13}C δ_{obs} for C-4 *vs.* molar ratio of Na^+ : $\mathbf{IC_a}$. This indicates multiple (4 : 1) complexation of the Na^+ within the macrocycle of the ion channel.

coordination of the nitrogen atom with cations.[15,30–32] The ion channel under investigation contains two anthracene units as lipid anchors and as fluorescent markers. Excitation at 363 nm gave rise to the characteristic anthracene emission spectrum with three maxima in the range 390–450 nm. The emission intensity, however, was reduced substantially and a comparison between $\mathbf{IC_a}$ and $\mathbf{IC_c}$ showed that quenching was due to PET from the lone pairs of the macrocyclic nitrogen atoms (with a possible contribution from the carbonyl groups) rather than the ferrocene unit. When the ion channel, as a 10^{-5} M solution in acetonitrile, was titrated with Na^+ ion, fluorescence emission increased in intensity over a ratio of 1–10 (Na^+ : IC) by a factor of 6 (Fig. 3) with a maximum being reached at a molar ratio of *ca.* 4 : 1 (see Fig. 4). Incidentally, similar results were obtained for K^+, Mg^{2+} and Ca^{2+} although with Ca^{2+}, the maximum change in intensity was a factor of about 40 rather than 6 indicating stronger coordination of trivalent nitrogen with $Ca^{2+}$and a consequent increase in fluorescence intensity. Thus the fluorescence experiments confirm the ^{13}C NMR spectroscopy findings suggesting coordination of 3–4 Na^+ ions within the overall channel structure.

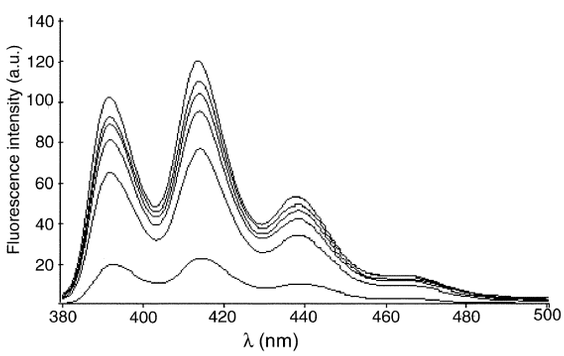

Fig. 3 Fluorescence emission intensity of ($\mathbf{IC_a}$) (10^{-5} M) as a function of added $NaSO_3CF_3$ in MeCN (RT, $\lambda_{exc.}$ = 363 nm). $NaSO_3CF_3$ (10^{-5} M): 0, 1, 2, 3, 4 and 10; increasing intensity from 0 to 10.

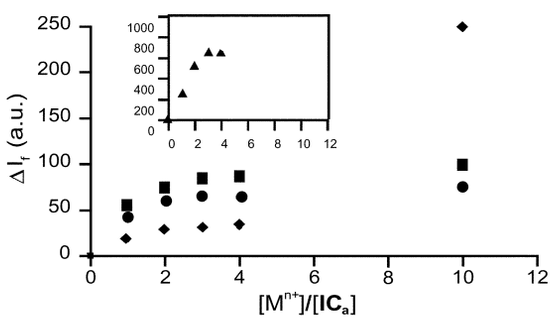

Fig. 4 Titration of ($\mathbf{IC_a}$, 10^{-5} M) with Na^+ (●), K^+ (■), Mg^{2+} (◆) and Ca^{2+} (▲) (inset) in MeCN. $\lambda_{exc.}$ = 363 nm, $\lambda_{em.}$ = 414–421 nm. (Note: For a ten molar excess in Mg^{2+} there is an unusually large ΔI_f which is most likely due to an accompanying conformational change of the ion channel.)

Cation binding by cyclic voltammetry

Both ferrocene-containing ion channels ($\mathbf{IC_{a,b}}$) exhibited irreversible oxidation waves for Fe^{2+}/Fe^{3+} at *ca.* 720 mV (*vs.* Ag/Ag^+) in both acetonitrile and dichloromethane and over a sweep rate range from 50–1000 mV s^{-1}. This is illustrated for $\mathbf{IC_b}$ in Fig. 5A in comparison with the reversible CV wave for **3** (from Fig. 1) that occurs at a significantly higher (50 mV) potential. Reversible cyclic voltammetry is the normal behaviour experienced with amide crown derivatives of ferrocene.[33,34] The anomalous behaviour of the ion channel is therefore attributed to the tertiary nitrogen atoms on the outer rings in relatively close proximity to the ferrocene unit. It seems likely that the tertiary nitrogen atoms of the flexible outer macrocycles stabilize the ferrocenium cation, possibly by electron transfer so that on the return (cathodic) sweep the corresponding reduction of the ferrocenium ion is not observed. Complexation of $\mathbf{IC_{a,b}}$ with cations induces the expected anodic shift and at higher concentrations, especially with divalent cations (*e.g.* Mg^{2+} or Ca^{2+}) reversibility of the ferrocene wave is re-established (Fig. 5B) presumably due to inhibition of electron transfer from trivalent nitrogen.[35] Both synthetic channels showed anodic shifts on complexation with cations and the results with Na^+ are shown in Table 3. The data suggest, in agreement with the NMR spectroscopy and fluorescence data, that the channels form 3 or 4 : 1 cation : ion channel complexes. However, the fact that the shifts are generally small (30–60 mV) and only one CV wave was observed in each case suggests weak binding and little influence on the ferrocene oxidation potential. Weak binding is, of course, a prerequisite for channel activity since strong binding ($K > 10^4$) would simply block the channel by prohibiting release from the binding site.

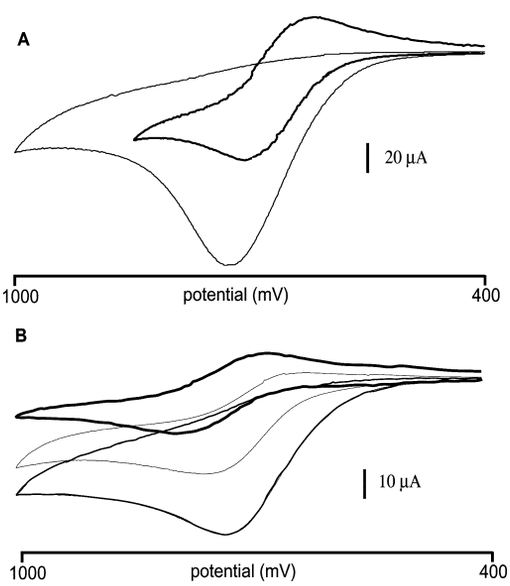

Fig. 5 A) Voltammetric response of; (thin line) 5 mM $\mathbf{IC_b}$; (thick line) 5 mM **3**. Solvent system: MeCN–0.2 M TBAP; scan rate: 50 mV s^{-1}. B) Voltammetric response of; (medium line) 3 mM $\mathbf{IC_b}$; (thin line) + 1 equivalent Mg^{2+}; (thick line) + 10 equivalent Mg^{2+}. Solvent system: MeCN–0.2 M TBAP; scan rate: 50 mV s^{-1}.

Cation flux using black lipid membrane preparations

We used a black lipid membrane preparation to generate the initial evidence that $\mathbf{IC_a}$ was functioning as an ion channel. Phosphatidylethanolamine (PE) planar bilayers were painted across a 200 μm diameter aperture in a septum dividing two aqueous compartments filled with 600 mM KCl, 10 mM HEPES, pH 7.2. The transport of K^+ ions was monitored across the bilayer after the addition of $\mathbf{IC_a}$ to give a final concentration of 17 nM of the synthetic ion channel. Typically

Table 3 Electrochemical oxidation potentials for compounds $\mathbf{IC_a}$ and $\mathbf{IC_b}$ with added $NaSO_3CF_3$

Ratio [a]	Oxidation potential, E_o/mV [b]	
	$\mathbf{IC_a}$	$\mathbf{IC_b}$
0 : 1	715	725
1 : 1	740	[c]
2 : 1	755	760 [d]
3 : 1	765 [d]	785 [d]
4 : 1	765 [d]	775 [d]
10 : 1	730 [d]	760 [d]

[a] Molar ratio $NaSO_3CF_3$ to crown. [b] Obtained in acetonitrile solution containing 0.2 M TBAP as supporting electrolyte. Solutions were 3 mM (for $\mathbf{IC_a}$) and 5 mM (for $\mathbf{IC_b}$). Oxidation potentials were determined with reference to Ag/Ag^+. Scan rate = 50 mV s^{-1}. [c] Data not recorded. [d] Broadening observed, oxidation potential imprecise.

there was a time delay of *ca.* 30 min prior to the observations of robust channel activity. Voltage steps (10 mV) from −40 to +70 mV across the bilayer revealed single open level transitions varying in lifetime from 50 ms to 20 s (Fig. 6A) with a mean conductance of 61 pS (Fig. 6B). The current-voltage response indicated non-Ohmic behaviour since the conductance on the anodic side was slightly less than that on the cathodic side (Fig. 6B). This result was qualitatively similar to that found by the patch clamp technique using $\mathbf{IC_b}$.[14] Further black lipid membrane studies will be described in later publications. Suffice it to say that our initial results indicated that $\mathbf{IC_a}$ did indeed exhibit ion channel properties and supported cation flux across the bilayer.

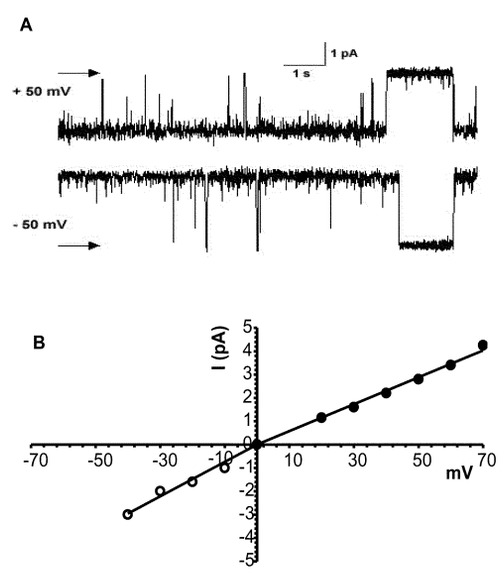

Fig. 6 A) Typical planar bilayer traces for 10 pmol $\mathbf{IC_a}$ at + 50 mV (top trace) and 10 pmol $\mathbf{IC_a}$ at −50 mV (bottom trace) using symmetrical KCl conditions (600 mM, 10 mM HEPES, pH 7.2). The arrows at the left hand side of the traces indicate the current level of the *closed* state. B) Current–voltage relationships for planar lipid bilayer studies of 10 pmol ($\mathbf{IC_a}$) using symmetrical KCl conditions (600 mM, 10 mM HEPES, pH 7.2). The average single channel conductance was 61 pS through the voltage range. There was a slight indication of non-Ohmic behaviour as demonstrated by the different slopes of the linear fits at negative and positive membrane potentials.

All the evidence above serves to illustrate that the artificial channels bind cations (Na^+, K^+, Mg^{2+} and Ca^{2+}) and offer a mechanism for transport through both natural and artificial (black lipid) membranes. However, it tells us little about the cumulative rate of transport, so this problem was addressed using the elegant ^{23}Na NMR method developed in model vesicle systems by Pike *et al.*,[20] Riddell,[21] and Hunt.[22]

Table 4 Observed linewidths (LW) of the Na_{IN} peak *vs.* [monensin] in vesicle solution together with the corresponding rate constants (k_{obs}) for Na^+ exchange; average of two measurements at each concentration of monensin

$10^5 \times$ [mon]	LW (Na_{IN})	LW (Na_{OUT})	k_{obs}/s^{-1} [a]
0.0	32.9	19.1	—
2.67	37.2	19.1	12.9
5.34	51.6	19.1	58.7
8.01	60.0	19.6	80.3

[a] Normalized to the line width (LW) of the Na_{OUT} peak. Linear regression of k_{obs} *vs.* [monensin] gives $k_2 = 1.04 \times 10^5$ l mol^{-1} s^{-1}.

Cation flux in unilamellar vesicles by ^{23}Na NMR spectroscopy

Unilamellar vesicles were prepared by the dialytic detergent removal technique[36] reported to give a spread of vesicle diameters between 200 and 600 nm. In each experiment a small volume of the vesicle suspension (0.75 ml, see Experimental) was treated with 3 µl of a 1 M aqueous solution of $DyCl_3$. The Dy(III) in the form of the $[Dy(PPP_i)_2]^{7-}$ complex ion induced a 6–10 ppm upfield shift of the extravesicular sodium NMR signal. The resulting NMR spectrum consisted of two unique and separate intra- and extravesicular Na^+ signals (see Fig. 7). The integration revealed a consistent (10–14%) encapsulation of intravesicular sodium.

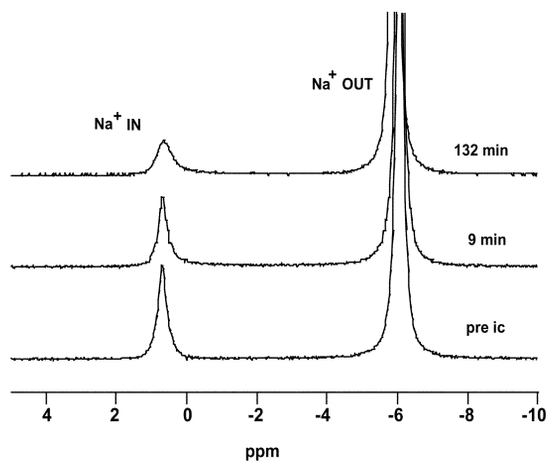

Fig. 7 ^{23}Na NMR spectra of a single vesicular suspension containing 3.0 µl of 1 M $DyCl_3$. Bottom spectrum was taken prior to, middle one 9 min after and top one 132 min after the addition of 2 µl of 5 mM $\mathbf{IC_a}$ in methanol at 291 K.

In order to analyze the dynamic exchange of Na^+ through the vesicles, we monitored the broadening of the intravesicular Na^+ signal in the presence of the antibiotic monensin and of our ion channel $\mathbf{IC_a}$. The study of monensin-mediated sodium transport was conducted to verify our technique and protocol. A vesicle sample was titrated with increasing aliquots (1–3 µl) of 20 mM monensin in methanol. The rates of Na^+ flux were extracted from the broadened intravesicular linewidth using the established procedure of Riddell and co-workers.[21a] The results, shown in Table 4, were compared to available literature data. A plot of k_{obs} *vs.* [monensin] was linear and gave $k_2 = 1.04 \times 10^6$ l mol^{-1} s^{-1} for a 200 mM Na^+ gradient compared to the literature value of 1.02×10^6 l mol^{-1} s^{-1}.[21a] Therefore, the vesicles and our protocol are comparable with other standard preparations, enhancing the validity of subsequent data derived using $\mathbf{IC_a}$.

The synthetic ion channel experiments were set up in a similar fashion, and were carried out in separate vesicles samples using µl quantities of 5 mM $\mathbf{IC_a}$ in a methanol solution. Upon addition of $\mathbf{IC_a}$, a broadening of the intravesicular sodium peak was always observed with a time dependency for the magnitude of the broadening. The ^{23}Na-NMR spectra in Fig. 7 show the

effect of the addition of 2 μl of $\mathbf{IC_a}$ (final ion channel concentration of 13.2 μM) on the intravesicular sodium signal's linewidth prior to, 9 minutes and 132 minutes after the ion channel addition. Using $\mathbf{IC_a}$ at a final concentration of 33.1 μM Fig. 8 plots the values of the extracted rates with time, revealing a maximum rate after *ca.* 30 min. An incubation period (at 60 °C) was observed in a ^{23}Na NMR investigation of gramicidin-induced ion transport through membranes under equilibrium conditions,[37] similar to the time-dependency for $\mathbf{IC_a}$ activity observed in our planar lipid bilayer and vesicle experiments.

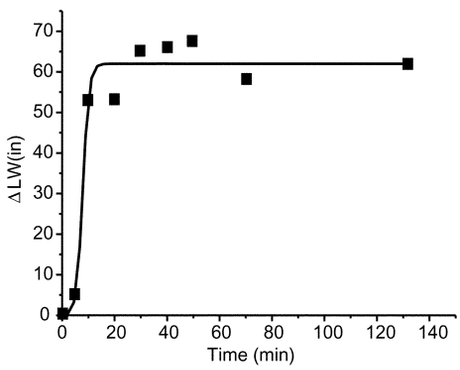

Fig. 8 Time dependence of linewidth broadening (ΔLW(IN)) upon addition of 5 μl of $\mathbf{IC_a}$ (5 mM) to a standard vesicle preparation.

A typical set of spectra for a dose–response (final concentrations of 3.3, 6.6, 13.2, 19.1 and 33.1 μM $\mathbf{IC_a}$) study is shown in Fig. 9 with all the applications showing similar time-dependency (*i.e.* broadening often reaching a plateau after ~1 h). Table 5 shows resulting linewidths and calculated rates of sodium transport (k_{obs}) for all the given concentrations. A plot of k_{obs} *vs.* [$\mathbf{IC_a}$] was linear (Fig. 10) giving a k_2 value of 5.9×10^6 l mol^{-1} s^{-1}. This is approximately six times faster than the k_2 value for monensin determined using the same [Na^+] gradient.[21a] Riddell reported that the k_2 values for monensin decreased with increasing [NaCl], a dependency that has yet be tested for $\mathbf{IC_a}$.

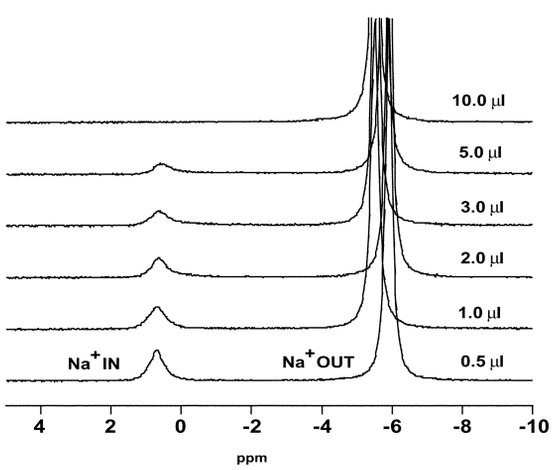

Fig. 9 ^{23}Na NMR spectra of vesicular suspensions containing 3.0 μl of 1 M $DyCl_3$ two hours after the addition of increasing amounts (0.5, 1.0, 2.0, 3.0, 5.0 and 10.0 μl) of 5 mM ion channel ($\mathbf{IC_a}$) in methanol at 291 K.

It might be expected that the transport rate for $\mathbf{IC_a}$ would reach a maximum as the vesicles become saturated. In fact there is an *indication* that the rate declines at higher concentrations of $\mathbf{IC_a}$ since the rate using 66.2 μM $\mathbf{IC_a}$ (after 6 min) is lower than expected from the linear regression line in Fig. 10. However, the k_2 values are nominal since we do not know what proportion of the ion channel in solution is incorporated into vesicle membranes. Also, a strict comparison of the rate found for $\mathbf{IC_a}$

Table 5 Observed linewidths (LW) of the Na_{IN} peak *vs.* [$\mathbf{IC_a}$] together with the corresponding rate constants (k_{obs}) for Na^+ exchange

$10^6 \times$ [IC]	Time (min)	LW(Na_{IN})	LW(Na_{OUT})	k_{obs}/s^{-1} [a]
	0	35.7	20.6	
3.3	5	37.9	20.4	
3.3	128	47.5	22.7	23.3
	0	40.2	25.5	
6.7	6	41.0	23.6	
6.7	132	56.3	25.8	48.5
	0	30.5	19.7	
13.3	9	34.8	19.5	
13.3	132	55.9	20.9	69.7
	0	38.6	21.5	
20.0	5	42.8	20.9	
20.0	132	76.3	20.7	127.7
	0	33.3	20.3	
33.3	7	38.2	20.2	
33.3	132	95.4	20.0	199.6

[a] Normalized to the line width (LW) of the Na_{OUT} peak.

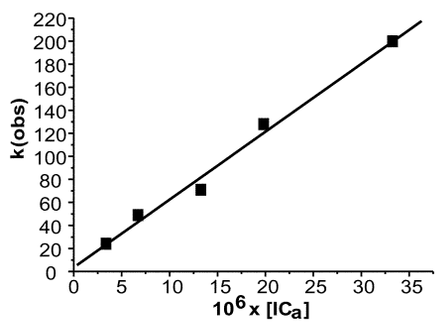

Fig. 10 Plot showing the linear relationship between k_{obs} and [$\mathbf{IC_a}$] yielding a k_2 value of 5.9×10^6 l mol^{-1} s^{-1}.

with that produced by gramicidin (another ion channel) is not feasible since the latter rate was found to be second order in [gramicidin].[37]

A few further observations are worth mentioning. Upon addition of $\mathbf{IC_a}$, the amount of intravesicular sodium was shown by integration to decrease with time, a decrease that was dependent on the amount of ion channel added. Thus, with 3.3 μM of $\mathbf{IC_a}$ the % Na_{IN} decreases from 14.5% to 11.5% over 2 h, whereas with 33.1 μM of $\mathbf{IC_a}$ it decreases from 14.8% to 3.6%. After introducing 66.2 μM $\mathbf{IC_a}$ to the vesicle sample, there was no detectable intravesicular sodium after 2 h (thus the only rate available for the 10 μl sample was calculated from the data at 6 min after mixing). This initially suggested that high concentrations of $\mathbf{IC_a}$ caused the vesicles to become 'leaky' and finally rupture. However, the rupture of the vesicles would create an immediate and proportional increase in the amount of extravesicular sodium integrated. This was not the case for the majority of the samples with the exception of the 66.2 μM $\mathbf{IC_a}$ where a complete disappearance of the intravesicular signal into the baseline only caused a slight 3% increase in the extravesicular integration. In any case, the flattening of the intravesicular signal does correlate with the expected bandshape pattern for intermediate exchange in an uncoupled two-site system where the two sites, Na_{IN} and Na_{OUT}, are unequally populated.[38]

Another interesting spectral feature was the appearance of a shoulder upfield of the intravesicular sodium peak upon addition of higher $\mathbf{IC_a}$ concentrations (>33.1 μM) This may be interpreted as appearance of a new resonance signal corresponding to a slight influx of the $[Dy(PPP_i)_2]^{7-}$ ion through the vesicular membrane. This effect has been previously observed and confirmed by Duval *et al.* in a study of ionophoric activity of the antibiotic peptaibol.[21c]

One of the novel aspects of the design of this ion channel is the inclusion of a ferrocene redox-active centre to act as a

mechanism for the regulation of ion flux. We performed a series of experiments in which we oxidized $\mathbf{IC_a}$ to investigate the potential of the redox-active centre to modify channel conductance. An aqueous solution of $\mathbf{IC_a}$ was prepared (5 mM) and treated with an equimolar amount of cerium(IV) ammonium nitrate. Oxidation of 2 μl of $\mathbf{IC_a}$ with Ce^{4+} prior to introduction into the vesicle suspension eliminated the ion channel activity over a monitoring period of 2 h. A 4-fold reduction in activity was also observed after oxidising 5 μl of $\mathbf{IC_a}$ with an equimolar concentration of OXONE® (potassium peroxymonosulfate) prior to addition to the vesicle mix. These exciting results demonstrate the ability of the ferrocene unit to regulate the function of this synthetic ion channel as the ferric ion may inhibit Na^+ transport by charge repulsion. Alternatively, the oxidized ion channel may not efficiently incorporate into the vesicle membrane. In an attempt to address the latter, we added oxidising agents to vesicles that had been previously exposed to $\mathbf{IC_a}$. An equimolar amount of cerium(IV) ammonium nitrate (to $\mathbf{IC_a}$) had no effect on the broadened bandwidth of the intravesicular sodium peak. Addition of an excess (10–35-fold) of Ce^{4+} caused the intra- and extravesicular sodium peaks to coalesce suggesting that this treatment oxidised the dysprosium complex. In preliminary experiments, a 10-fold molar equivalent of OXONE® slightly reduced (by ~15%) the peak broadening achieved after addition of 5 μl $\mathbf{IC_a}$to the vesicle mix. The potential of the redox-centre to act as a molecular 'switch' for ion channels incorporated in vesicular membranes will be explored in future studies by alternating additions of oxidising and reducing agents. However, to date we have shown that oxidation of the ferrocene moiety inhibits the transmembrane transport of Na^+, and have demonstrated the effectiveness of including a ferrocene centre for controlling conductance within a synthetic ion channel.

Conclusion

Spectroscopic and cyclic voltammetry studies suggest that the synthetic, redox-active ion channel ($\mathbf{IC_a}$) coordinates 3–4 cations to afford a 'billiard ball' mechanism of ion transport analogous to that found with natural protein channels. This study has also shown that $\mathbf{IC_a}$ conducts Na^+ ions through lipid bilayers at a rate that is approximately six times faster than the ionophore, monensin. Oxidation of the ferrocene unit within the channel inhibits the ion transport, demonstrating the potential role of a redox-active centre in regulating transmembrane cation flux.

Experimental

^{1}H and ^{13}C NMR measurements

^{1}H-NMR and ^{13}C-NMR spectra were recorded on Bruker AM-360 or Bruker AMX-400 spectrometers operating at 360.13 MHz or 400.1 MHz for ^{1}H and 90.6 MHz or 100.6 MHz for ^{13}C-NMR respectively. ^{1}H-NMR chemical shifts (δ) are given in ppm downfield from tetramethylsilane (TMS) as internal standard with the following abbreviations for peak multiplicity, br = broad, s = singlet, d = doublet, t = triplet, q = quartet, qu = quintet, m = multiplet. Chemical shifts in ^{13}C-NMR were referenced to the $CDCl_3$ signal at 77.1 ppm in $CDCl_3$. ^{13}C-DEPT spectra were recorded using the 135° pulse sequence, giving positive signals for CH_3 and CH, negative signals for CH_2 {indicated by (+) or (−) respectively} and no signal for quaternary (*ipso*) carbon atoms.

^{23}Na NMR measurements

Sodium cation flux was measured following the ^{23}Na NMR method of Riddell *et.al.* [21b] ^{23}Na NMR spectroscopic measurements were performed on a JEOL Eclipse 400 NMR spectrometer with sodium observation at 105 MHz. A 5 mm tunable probe was used with the following acquisition parameters: tip angle 57°; sweep width ± 11000 Hz; relaxation delay = 0.5 s; number of spectral points = 4K; locked mode (D_2O). Each spectrum represents a collection of 200 scans Fourier transformed with an exponential line broadening of 0.2 Hz. NMR samples were prepared by mixing 675 μl of vesicular suspension, 75 μl of 100 mM NaCl–20 mM $Na_5P_3O_{10}$ in D_2O and 3.0 μl of 1 M $DyCl_3$ to obtain a sodium spectrum consisting of the intravesicular resonance separated from the extravesicular resonance by at least 6 ppm. All spectra were recorded at 291 K. Relaxation times (T_1) for the sodium signals were measured to be ~0.035 s. Linewidth measurements were obtained by deconvolution of the Na^+ resonance signals by a JEOL Lorentzian bandshape fit.

Synthesis characterization

High resolution mass spectrometry data were collected using fast-atom-bombardment (HRMS-FAB) which was performed at the ULIRS Mass Spectrometry Facility, School of Pharmacy, London, on a VG ZAB-SE instrument using VG Opus software (resolution 8–10K). Infrared spectra were recorded on a Perkin-Elmer Paragon 1000 FT-IR spectrometer using NaCl plates (neat) or KBr discs. Thin layer chromatographic (TLC) analyses used aluminium oxide 60 F_{254} neutral on aluminium sheets with a 0.2 mm layer thickness, (Merck) with 5% MeOH–CH_2Cl_2 as eluent. Preparative chromatography columns were packed with alumina [neutral, type 507C, Fluka, (0.05–0.15 mm; pH 7.0 ± 0.5)], or silica gel 60 (F_{254}, 0.035–0.070 mm, Merck).

Solvents were purified by standard procedures and were stored under nitrogen over molecular sieves (4–8 mesh).

Tetrabutylammonium perchlorate (TBAP) was purchased from Fluka and used without further purification. All the metal trifluoromethanesulfonates (triflates) except $Ca(SO_3CF_3)_2$ were used as obtained from Aldrich.

Preparation of calcium trifluoromethanesulfonate

Trifluoromethanesulfonic acid (0.89 g, 5.92 mmol) dissolved in dry MeCN (1 ml) was added to a suspension of $CaCO_3$ (0.3 g, 2.96 mmol) in dry MeCN (4 ml) with stirring. Additional dry MeCN was added with warming to aid dissolution. After 15 min a trace amount of insoluble starting material was filtered off and the filtrate was evaporated to dryness. The product was dried under vacuum (130 °C, 6.0–7.0 × 10^{-2} mbar) for 2 h to give a white crystalline solid (0.71 g, 64%).

Electrochemical experiments

Electrochemical experiments were performed with an EG&G Princeton Applied Research Versastat™ potentiostat and the current–potential traces analysed using EG&G 270/250 Research Electrochemistry Software. Cyclic voltammetry data were recorded using a glassy carbon working electrode (diameter, 0.3 cm), a platinum counter electrode and a Ag/AgCl reference electrode (at 0.222 V). The glassy carbon electrode was polished with alumina between recordings. The acetonitrile solution, containing 0.2 M TBAP as supporting electrolyte, 3.0–5.0 mM of the ligand and variable concentrations of metal triflates, was placed in an unsealed one-compartment cell and degassed by bubbling with argon prior to each recording. Addition of the metal triflates was accompanied by stirring but measurements were made on the unstirred solutions and experiments were conducted at room temperature under argon.

^{13}C NMR titration experiments

Chemical shifts (δ_{obs}) were recorded as a function of the changing concentration of $NaSO_3CF_3$ at constant ligand concentration. The ion channel ($\mathbf{IC_a}$, 41 mg, 0.02 mmol) was dissolved in CD_3CN (0.5 ml), and the ^{13}C NMR spectra

recorded after each addition of $NaSO_3CF_3$. Titration curves were obtained by plotting the observed chemical shift, δ_{obs} against the concentration ratio, [$NaSO_3CF_3$]/[ligand].

Fluorescence methods

Fluorescence spectra were measured with a Perkin-Elmer Luminescence Spectrometer LS50B and analyzed with FL WinLab Version 2.01 Software using either the default scan or time drive methods. The excitation and emission slits were 10 nm and 2.5 nm respectively. Fluorescence intensities of the ligands (10^{-5} M) excited at 363 nm were measured in acetonitrile at room temperature. The titrations were conducted by progressively adding the metal salts, injected as concentrated solutions, to a cuvette containing the ligand solution (2.5 ml). Samples were shaken briefly prior to each recording and the added equivalents of cation were plotted against the emission-intensity change in the 414–421 nm region.

Ion channel recordings: black lipid membrane experiments

Standard black lipid membrane techniques were employed to record synthetic ion channel activity in planar lipid bilayers. Phospholipid membranes were formed by the painted bilayer method.[39] Phosphatidylethanolamine (Avanti Polar Lipids, Birmingham, AL, USA) was stored as a chloroform dispersion at −80 °C in sealed glass vials. **IC_a** was stored in DMSO at −20 °C prior to use. Electrolyte solutions in distilled water consisted of 600 mM KCl, 10 mM HEPES, titrated to pH 7.2 with KOH and stored at 4 °C. The lipid solution was prepared by evaporating off the chloroform from the stock solution under a stream of nitrogen, before dispersal in n-decane (35 mg ml^{-1}). This solution was used to pre-treat the aperture in a bilayer cup (a polystyrene copolymer). The dispersion was spread using a 'painting stick' fashioned from a plastic Pasteur pipette. The stick was dipped in the liquid dispersion and a small quantity painted across the 200 μm-diameter hole in the cup and allowed to dry. The KCl solution was added to both cup (referred to as *cis*, volume 0.6 ml) and the block chambers (*trans*, volume 4 ml). Each chamber was connected *via* an agar bridge to a Ag/AgC1 electrode placed in separate electrode wells (containing 4 M LiCl). The whole apparatus was enclosed in a grounded Faraday cage seated on a metal base plate resting on an air-cushioned table.

The painting stick was again dipped in the lipid–decane solution, and the lipid was then painted across the aperture in the cup. Square wave pulses (4 mV) were applied to the *cis* chamber to monitor membrane formation with the *trans* chamber held at virtual ground. Bilayer formation was detected by the disappearance of the square wave and the appearance of a capacitance spike. With thinning of the lipid film over the hole, the height of the spike increased to a maximum signifying stable bilayer formation. Thinning usually occurred with 1–10 min and the final capacitance of the bilayers was typically 60–120 pF. The aqueous solution in the cup holder was stirred, and 0.1–5 μl of a 10 μM **IC_a** solution (in DMSO) was added to the *cis* chamber (final concentration of **IC_a** of 1.7–82.6 nM). When varying holding potentials were applied, current flow across the bilayer was measured using an operational amplifier as a current–voltage converter. Single-channel fluctuations were displayed on an oscilloscope (Gould Digital Storage Oscilloscope OS4020) and stored on digital audio tape (Biologic DTR 1203 recorder. For analysis, data were replayed, filtered with an 8-pole Bessel filter (Model 900, Frequency Devices) and sampled using Satori V3.2 software on a dedicated PC. Data were filtered at 100 Hz and sampled at 200 Hz. All experiments were carried out at room temperature.

Preparation of unilamellar vesicles from egg phosphatidylcholine by detergent dialysis

Unilamellar vesicles were prepared from egg yolk phosphatidylcholine using a modified detergent dialysis technique.[21a] A sample of grade 1 lecithin (50 mg) in chloroform–methanol (Lipid Products, Redhill, Surrey, UK) was evaporated under N_2 and then dissolved in a solution (3 ml) containing 200 mM NaCl, 5 mM MES (pH: 6.5) and 300 mM, n-octyl-β-D-glucopyranoside (Calbiochem). The lipid solution was pipetted into a 6 mm diameter cellulose membrane dialysis tubing, and dialysed against 2.5 l of the external solution containing 200 mM NaCl, 5 mM MES (pH, 6.5) at room temperature. External solutions were pre-equilibrated, continually bubbled with N_2 throughout dialysis, and were changed every 10–12 h with three solution exchanges. Then, in a final 8 h dialysis, the external solution was exchanged for 2.5 l of a deoxygenated solution containing 100 mM NaCl, 20 mM Na-tripolyphosphate, 50 mM choline chloride and 5 mM MES (pH: 6.5). The vesicle suspension was then carefully pipetted out of the dialysis bag and used immediately.

Preparation of the ion channel (IC_a)

***N*-*tert*-Butoxycarbonyl-diaza-18-crown-6.**

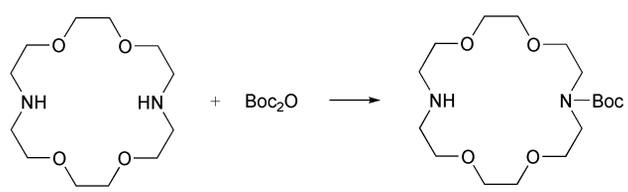

4,13-Diaza-18-crown-6 (5.96 g, 22.70 mmol) was dissolved in dioxane (130 ml) and warmed with stirring at 40 °C to aid dissolution. A solution of di-*tert*-butyl dicarbonate (4.97 g, 22.70 mmol) in dioxane (70 ml) was added during 5 min and the mixture was stirred at 40 °C for 30 min and for a further 16 h at RT. The mixture was concentrated *in vacuo* and ether (30 ml) was added. Unreacted 4,13-diaza-18-crown-6 precipitated as a white solid (1.46 g, 25%) which was filtered off and the filtrate was concentrated *in vacuo*. Column chromatography (alumina) gave two major products. The first fraction (0–0.5% MeOH–CH_2Cl_2) gave *N*,*N*′-di-*tert*-butoxycarbonyl-diaza-18-crown-6 as a colourless oil (2.20 g, 22%) that solidified on standing. The second fraction (0.5–1.5% MeOH–CH_2Cl_2) gave the product, *N*-*tert*-butoxycarbonyl-diaza-18-crown-6 as a pale yellow oil (3.60 g, 44%). ^{1}H-NMR ($CDCl_3$) δ 1.45 [s, 9H, $(CH_3)_3COC(O)$], 2.76 (br-s, ^{1}H, N*H*), 2.81 (t, 4H, J = 4.6 Hz, NCH_2CH_2O), 3.51 (t, 4H, J = 5.6 Hz, $OC(O)NCH_2$), 3.55–3.65 (m, 16H, $CH_2OCH_2CH_2OCH_2$); ^{13}C-NMR ($CDCl_3$) δ 28.5(+), 47.2(−), 47.5(−), 49.3(−), 69.6(−), 69.9(−), 70.0(−), 70.2(−), 79.4, 155.5; HRMS-FAB for $C_{17}H_{35}N_2O_6$, M_{calcd} 363.2495; M_{obs} 363.2505; IR (neat): 3455 (br, OH from H_2O/NH), 2870 (CH), 1695 (C=O), 1480, 1460, 1410, 1365, 1290, 1245, 1155, 1120, 1080 cm^{-1}.

***N*-(9-Anthrylmethyl)-*N*′-*tert*-butoxycarbonyl-diaza-18-crown-6.** A solution of *N*-*tert*-butoxycarbonyl-diaza-18-crown-6 (2.00 g, 8.29 mmol) and 9-chloromethylanthracene (1.25 g, 5.51 mmol) in butyronitrile (43 ml) was heated under reflux for 24 h in the presence of anhydrous Na_2CO_3 (11.70 g, 110.0 mmol) and KI (0.12 g, 0.68 mmol). The mixture was allowed to cool, filtered and concentrated *in vacuo*. The yellow residue was redissolved in CH_2Cl_2 (30 ml), washed with water (3 × 30 ml), dried ($MgSO_4$) and concentrated *in vacuo*. The product was obtained by column chromatography (alumina, 0.4–0.5% MeOH–CH_2Cl_2) as a bright orange oil (2.14 g, 71%). ^{1}H-NMR ($CDCl_3$) δ 1.45 [s, 9H, $(CH_3)_3COC(O)$], 2.88 (br-t, 2H, J = 5.4 Hz, NCH_2CH_2O), 2.93 (br-t, 2H, J = 6.1 Hz, NCH_2CH_2O), 3.48–3.64 (m, 20H, $CH_2OCH_2CH_2OCH_2$, $OC(O)NCH_2$), 4.58 (s, 2H, anthracene-CH_2N), 7.41–7.52 (m, 4H), 7.97 (d, J = 8.8 Hz, 2H), 8.39 (s, ^{1}H), 8.53 (d, J = 8.8 Hz, 2H); ^{13}C-NMR ($CDCl_3$) δ 28.5(+), 48.0(−), 48.2(−), 52.0(−), 53.7(−), 53.9(−),

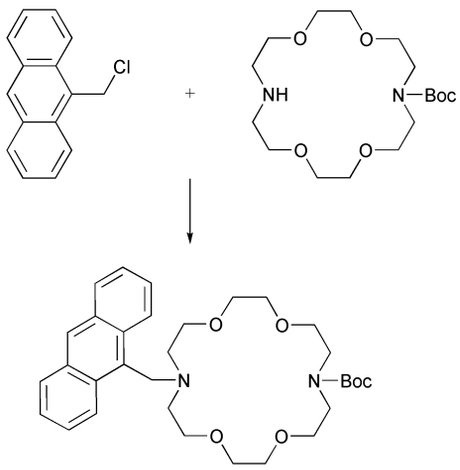

70.0(−), 70.2(−), 70.4(−), 70.5(−), 70.8(−), 70.8(−), 79.5, 124.9(+), 125.3(+), 125.6(+), 127.5(+), 129.0(+), 130.5, 131.4, 131.5, 155.6; HRMS-FAB for $C_{32}H_{45}N_2O_6$, M_{calcd} 553.3278; M_{obs} 553.3241; IR (neat): 3490 (br, OH from H_2O), 3050 (aromatic CH), 2865 (CH), 1690 (C=O), 1625, 1470, 1455, 1410, 1365, 1285, 1245, 1120 cm^{-1}.

***N*-(9-Anthrylmethyl)-diaza-18-crown-6.** *N*-(9-Anthrylmethyl)-

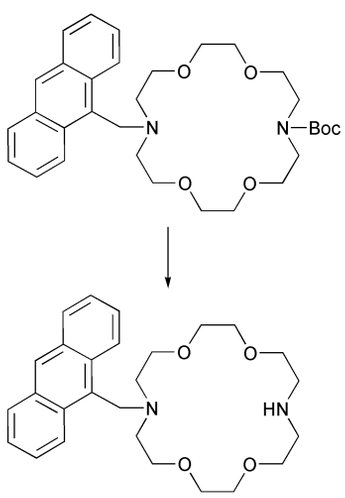

N′-tert-butoxycarbonyl-diaza-18-crown-6 (0.96 g, 1.74 mmol) was dissolved in a mixture of TFA (2 ml, 2.96 g, 25.96 mmol) and CH_2Cl_2 (8 ml) and stirred at RT for 16 h. The solution was concentrated *in vacuo*, redissolved in CH_2Cl_2 (20 ml), washed with a Na_2CO_3 solution (10% w/v, 3 × 20 ml), dried ($MgSO_4$) and concentrated *in vacuo* to give an orange oil (0.76 g, 97%).^{1}H-NMR ($CDCl_3$) δ 2.61 (br-s, ^{1}H, N*H*), 2.81 (t, 4H, J = 4.8 Hz, NCH_2CH$_2$O), 2.89 (t, 4H, J = 5.6 Hz, NCH_2CH$_2$O), 3.52–3.64(m,16H,CH_2OCH_2CH_2OCH_2),4.60(s,2H,anthracene-CH_2N), 7.41–7.52 (m, 4H), 7.96 (d, J = 8.8 Hz, 2H), 8.38 (s, ^{1}H), 8.57 (d, J = 8.8 Hz, 2H); ^{13}C-NMR ($CDCl_3$) δ 49.1(−), 51.7(−), 53.5(−), 69.9(−), 70.0(−), 70.3(−), 70.8(−), 124.6(+), 125.2(+), 125.3(+), 127.1(+), 128.7(+), 130.5, 131.2 (2 peaks); HRMS-FAB for $C_{27}H_{37}N_2O_4$, M_{calcd} 453.2753; M_{obs} 453.2720; IR (neat): 3445 (br, OH from H_2O/NH), 3050 (aromatic CH), 2865 (CH), 1670, 1625, 1450, 1350, 1300, 1250, 1115 cm^{-1}.

***N*-(9-Anthrylmethyl)-*N′*-(10-bromodecyl)diaza-18-crown-6.** A solution of *N*-(9-anthrylmethyl)-diaza-18-crown-6 (0.76 g, 1.68 mmol) and 1,10-dibromodecane (1.51 g, 5.03 mmol) in butyronitrile (34 ml) was heated under reflux for 90 min under nitrogen in the presence of anhydrous Na_2CO_3 (5.26 g, 49.60 mmol) and KI (33 mg, 0.20 mmol). The mixture was allowed to cool, filtered and concentrated *in vacuo*. The orange residue was redissolved in CH_2Cl_2 (30 ml), washed with water (3 × 30 ml),

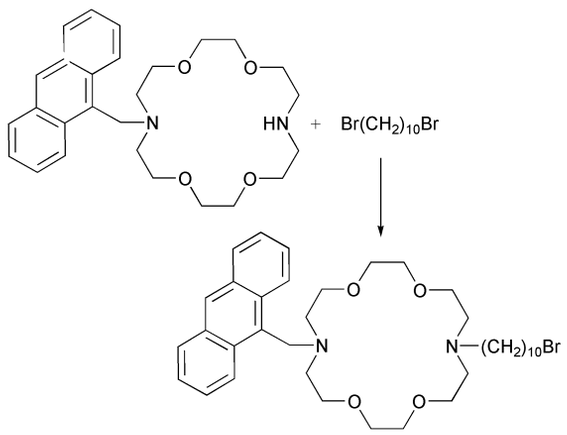

dried ($MgSO_4$) and concentrated *in vacuo*. The product was obtained by column chromatography (alumina, 0.4–0.5% MeOH–CH_2Cl_2) as an orange oil (0.63 g, 56%). ^{1}H-NMR ($CDCl_3$) δ 1.20–1.35 (br-s, 12H, alkyl), 1.41 (br-qu, 2H, NCH$_2$-CH_2CH$_2$), 1.84 (qu, 2H, J = 6.9 Hz, BrCH$_2$CH_2), 2.54 (br-s, 2H, NCH_2CH$_2$CH$_2$), 2.84 (br-s, 4H, NCH_2CH$_2$O), 2.90 (t, 4H, J = 5.8 Hz, anthraceneCH$_2$NCH_2CH$_2$O), 3.40 (t, 2H, J = 6.9 Hz, BrCH_2CH$_2$), 3.51–3.69 (m, 16H, CH_2OCH_2CH_2OCH_2), 4.58 (s, 2H, anthraceneCH_2N), 7.42–7.52 (m, 4H), 7.98 (d, 2H, J = 8.8 Hz), 8.39 (s, ^{1}H), 8.54 (d, 2H, J = 8.8 Hz); ^{13}C-NMR ($CDCl_3$) δ 27.5(−), 28.2(−), 28.8(−), 29.4(−), 29.5(−), 32.9(−), 34.1(−), 51.9(−), 53.5(−), 53.9(−), 70.2(−), 70.6(−), 70.8(−), 124.89(+), 125.3(+), 125.6(+), 127.5(+), 129.0(+), 130.5, 131.4, 131.5; HRMS-FAB for $C_{37}H_{35}BrN_2O_4Na$, M_{calcd} 693.3243; M_{obs} 693.3211; IR (neat): 3425 (br, OH from H_2O), 3050 (aromatic CH), 2925 (CH), 2855 (CH), 1670, 1625, 1465, 1445, 1350, 1285, 1250, 1115 cm^{-1}.

***N*-(9-Anthrylmethyl)-*N′*-[10-(*N′-tert*-butoxycarbonyl-diaza-18-crown-6)decyl]-diaza-18-crown-6.** A solution of *N*-(9-

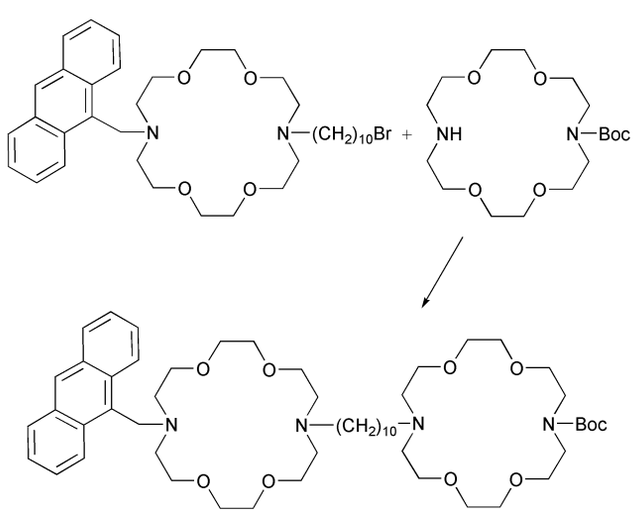

anthrylmethyl)-*N′*-(10-bromodecyl)-diaza-18-crown-6 (1.30 g, 1.94 mmol) and *N-tert*-butoxycarbonyl-diaza-18-crown-6 (0.70 g, 1.94 mmol) in butyronitrile (22.5 ml) was heated under reflux for 20 h under nitrogen in the presence of anhydrous Na_2CO_3 (4.10 g, 38.70 mmol) and KI (40 mg, 0.24 mmol). The mixture was allowed to cool, filtered and concentrated *in vacuo*. The yellow residue was redissolved in CH_2Cl_2 (40 ml), washed with water (3 × 40 ml), dried ($MgSO_4$) and concentrated *in vacuo*. The product was obtained by column chromatography (alumina, 0.4–0.8% MeOH–CH_2Cl_2) as an orange oil (1.29 g, 70%). ^{1}H-NMR ($CDCl_3$) δ 1.20–1.32 (br-s, 12H, alkyl), 1.40–1.50 (br-s, 13H, (CH_3)$_3$COC(O), NCH$_2$CH_2CH$_2$), 2.52 (br-s, 4H, NCH_2CH$_2$CH$_2$), 2.82 (br-s, 8H, NCH_2CH$_2$O), 2.90 (t, 4H, J = 5.8 Hz, anthraceneCH$_2$NCH_2CH$_2$O), 3.50 (t, 4H, J = 5.6

Hz, OC(O)NCH_2), 3.52–3.65 (m, 32H, CH_2OCH_2CH_2OCH_2), 4.59 (s, 2H, anthraceneCH_2N), 7.42–7.52 (m, 4H), 7.98 (d, 2H, J = 8.8 Hz), 8.39 (s, ^{1}H), 8.54 (d, 2H, J = 8.8 Hz); ^{13}C-NMR ($CDCl_3$) δ 27.5(−), 28.5(+), 29.6(−), 48.0(−), 48.1(−), 51.9(−), 53.5(−), 53.8(−), 56.0(−), 70.0(−), 70.2(−), 70.6(−), 70.8(−), 79.5(−), 124.9(+), 125.3(+), 125.6(+), 127.5(+), 129.0(+), 130.5, 131.4, 131.5, 155.6; HRMS-FAB for $C_{54}H_{89}N_4O_{10}$, M_{calcd} 953.6579; M_{obs} 953.6549; IR (neat): 3440 (br, OH from H_2O), 3050 (aromatic CH), 2925 (CH), 2855 (CH), 1695 (C=O), 1460, 1410, 1365, 1350, 1290, 1250, 1115 cm^{-1}.

***N*-(9-Anthrylmethyl)-*N′*-[10-(diaza-18-crown-6)decyl]-diaza-18-crown-6.** *N*-(9-Anthrylmethyl)-*N′*-[10-(*N′*-*tert*-butoxycarbonyl-diaza-18-crown-6)decyl]-diaza-18-crown-6 (1.20 g, 1.26 mmol) was dissolved in a mixture of TFA (3 ml, 4.44 g, 38.94 mmol) and CH_2Cl_2 (12 ml) and stirred at RT for 16 h. The solution was evaporated to dryness, redissolved in CH_2Cl_2 (30 ml), washed with a Na_2CO_3 solution (10% w/v, 3 × 30 ml), dried ($MgSO_4$) and concentrated *in vacuo* to give an orange oil (0.96 g, 90%).^{1}H-NMR ($CDCl_3$) δ 1.20–1.35 (br-s, 12H, alkyl), 1.43 (br-qu, 4H, NCH_2CH_2CH$_2$), 2.49 (m, 4H, NCH_2CH$_2$CH$_2$), 2.78 (t, 8H, J = 5.8 Hz, NCH_2CH$_2$O), 2.82 (t, 4H, J = 4.8 Hz, NCH_2CH$_2$O), 2.90 (t, 4H, J = 5.8 Hz anthraceneCH$_2$NCH_2-CH$_2$O), 3.53–3.65 (m, 32H, CH_2OCH_2CH_2OCH_2), 4.59 (s, 2H, anthracene (CH_2N)), 7.41–7.52 (m, 4H), 7.97 (d, 2H, J = 8.8 Hz), 8.39 (s, ^{1}H), 8.54 (d, 2H, J = 8.8 Hz); ^{13}C-NMR ($CDCl_3$) δ 26.9(−), 27.2(−), 27.5(−), 29.6(−), 49.2(−), 51.9(−), 53.7(−), 53.8(−), 53.9(−), 55.3(−), 56.1(−), 69.8(−), 70.0(−), 70.1(−), 70.3(−), 70.5(−), 70.8(−), 70.9(−), 124.8(+), 125.3(+), 125.5(+), 127.4(+), 128.9(+), 130.5, 131.4 (2 peaks); HRMS-FAB for $C_{49}H_{79}N_4O_8Na$, M_{calcd} 874.5796; M_{obs} 874.5827; IR (neat): 3440 (br, OH from H_2O/NH), 2925 (CH), 2855 (CH), 1670, 1460, 1350, 1285, 1120 cm^{-1}.

1,1′-Bis[*N*-carbonyl-*N′*-[10-(*N′*-(9-anthrylmethyl)-diaza-18-crown-6)decyl]-diaza-18-crown-6]ferrocene(IC$_a$).1,1′-Bis(chlorocarbonyl)ferrocene (33 mg, 0.11 mmol) in dry toluene (4 ml) was added dropwise over 5 min to a solution of *N*-(9-anthrylmethyl)-*N′*-[10-(diaza-18-crown-6)decyl]-diaza-18-crown-6 (0.18 g, 0.21 mmol) and dry Et_3N (22 mg, 0.21 mmol) in dry toluene (4 ml). The mixture was stirred at RT for 24 h under nitrogen, filtered and concentrated *in vacuo* to give an orange residue. The product was obtained by column chromatography (alumina, 0.8–1.5% MeOH–CH_2Cl_2) as an orange oil (0.13 g, 61%) that became a dark orange solid (mp >300 °C, dec) on drying under vacuum.

^{1}H-NMR ($CDCl_3$) δ 1.20–1.32 (br-s, 24H, alkyl), 1.46 (br-s, 8H, NCH$_2$CH_2CH$_2$), 2.54 (br-s, 8H, NCH_2CH$_2$CH$_2$), 2.82 (br-s, 16H, NCH_2CH$_2$O), 2.90 (t, 8H, J = 5.8 Hz, anthracene-CH$_2$NCH_2CH$_2$O), 3.50–3.85 (m, 72H, CH_2OCH_2CH_2OCH_2, C(O)NCH_2), 4.37 (t, 4H, J = 1.9 Hz, CpH), 4.58 (s, 4H, anthracene-CH_2N), 4.65 (t, 4H, J = 1.9 Hz, CpH), 7.42–7.52 (m, 8H), 7.98 (d, 4H, J = 8.8 Hz), 8.39 (s, 2H), 8.54 (d, 4H, J = 8.8 Hz); ^{13}C-NMR ($CDCl_3$) δ, 27.0(−), 27.5(−), 29.6(−), 47.6(−), 49.6(−), 51.9(−), 53.8(−), 56.0(−), 69.8(−, br), 70.2(−), 70.6(−), 70.7(−), 70.9(−), 71.8(+), 72.0(+), 80.1, 124.8(+), 125.3(+), 125.6(+), 127.5(+), 128.9(+), 130.5, 131.4, 131.4, 169.9; HRMS-FAB for $C_{110}H_{166}FeN_8O_{18}Na$, M_{calcd} 1966.1567; M_{obs} 1966.1691; IR (neat): 3435 (br, OH from H_2O), 2925 (CH), 2855 (CH), 1615 (amide C=O), 1470, 1415, 1350, 1285, 1110 cm^{-1}.

Acknowledgements

We would like to acknowledge Dr. David Bickar and Dr. Charles Amass, Department of Chemistry, Smith College for helpful advice on the vesicle preparations and on the sodium NMR spectroscopy. We would also like to thank the EPSRC for a postgraduate ROPA award (to G. J. K) and Professor A. J. Williams and Dr M. L. Bannister, Department of Cardiac Medicine, National Heart and Lung Institute, London, UK for provision and advice in the use of planar lipid bilayers equipment

References

1 D. J. Aidley and P. R. Stanfield, *Ion channels : molecules in action*, University Press, Cambridge, 1996.

2 W. D. Stein, *Channels, Carriers and Pumps*, Academic Press, New York, 1990.

3 (*a*) G. W. Gokel and A. Mukhopadhyay, *Chem. Soc. Rev.*, 2001, **30**(5), 274–286; (*b*) S. L. De Wall, E. S. Meadows, C. L. Murray, H. Shabbany and G. W. Gokel, *Supramol. Chem.*, 2000, **12**(1), 13–22; (*c*) H. Shabany, R. Ferdani and G. W. Gokel, *Supramol. Chem.*, 2001, **13**(3), 391–404.

4 (*a*) N. Voyer and M. Robitaille, *J. Am. Chem. Soc.*, 1995, **117**, 6599–6600; (*b*) J-C. Meillon and N. Voyer, *Angew. Chem., Int. Ed. Engl.*, 1997, **36**(9), 967–969.

5 S. Fernandez-Lopez, H.-S. Kim, E. C. Choi, M. Delgado, J. R. Granja, A. Khasonov, K. Kraehenbuehl, G. Long, D. A. Weinberger, K. M. Wilcoxen and M. R. Ghadiri, *Nature*, 2001, **412**, 452–456.
6 E. Abel, E. S. Meadows, I. Suzuki, T. Jin and G. W. Gokel, *Chem. Commun.*, 1997, 1145–1146.
7 C. L. Murray and G. W. Gokel, *Chem. Commun.*, 1998, 2477–2478.
8 H. Shabany and G. W. Gokel, *Chem. Commun.*, 2000, 2373–2374.
9 H. Shabany, C. L. Murray, G. W. Gokel, C. A. Gloeckner, M. A. Grayson and M. L. Gross, *Chem Commun*, 2000, 2375–2376.
10 C. L. Murray, H. Shabany and G. W. Gokel, *Chem. Commun.*, 2000, 2371–2372.
11 D. A. Dougherty and H. A. Lester, *Angew. Chem., Int. Ed. Engl.*, 1998, **37**, 2329–2331.
12 P. Schmitt, P. D. Beer, M. G. B. Drew and P. D. Sheen, *Angew. Chem., Int. Ed. Engl.*, 1997, **36**, 1840–1842.
13 P. J. Cragg, M. C. Allen and J. W. Steed, *Chem. Commun.*, 1999, 553–554.
14 C. D. Hall, G. J. Kirkovits and A. C. Hall, *Chem. Commun.*, 1999, 1897–1898.
15 A. P. de Silva and S. A. de Silva, *J. Chem. Soc., Chem. Commun.*, 1986, 1709–1710.
16 (*a*) S. L. De Wall, E. S. Meadows, L. J. Barbour and G. W. Gokel, *Chem. Commun.*, 1999, 1553–1554; (*b*) E. Abel, G. E. M. Maguire, O. Murillo, I. Suzuki, S. L. De Wall and G. W. Gokel, *J. Am. Chem. Soc.*, 1999, **121**, 9043–9052.
17 (*a*) K. Ho, C. G. Nichols, W. J. Lederer, J. Lytton, P. M. Vassilev, M. V. Kanazirska and S. C. Herbert, *Nature*, 1993, **362**, 31–38; (*b*) Y. Kubo, T. J. Baldwin, Y. N. Jan and L. Y. Jan, *Nature*, 1993, **362**, 127–133.
18 H. Plenio and C. Aberle, *Organometallics*, 1997, **16**(26), 5950–5957; H. Plenio and C. Aberle, *Chem.-Eur. J.*, 2001, **7**(20), 4438–4446.
19 J. D. Schmitt, M. S. P. Sansom, I. D. Kerr, G. G. Lunt and R. Eisenthal, *Biochemistry*, 1997, **36**, 1115–1122.
20 M. M. Pike, S. R. Simon, J. A. Balschi and C. S. Springer, *Proc. Natl. Acad. Sci.*, 1982, **79**, 810–814.
21 (*a*) F. G. Riddell and M. K. Hayer, *Biochem. Biophys. Acta*, 1985, **817**, 313–317; (*b*) F. G. Riddell and S. J. Tompsett, *Biochim. Biophys. Acta.*, 1990, **1024**, 193–197; (*c*) D. Duval, F. G. Riddell, S. Rebuffat, N. Platzer and B. Bodo, *Biochem. Biophys. Acta.*, 1998, **1372**, 370–378.
22 G. R. A. Hunt and J. A. Veiro, *Biochem. Soc. Trans.*, 1986, **14**, 602–603.
23 C. D. Hall, J. H. R. Tucker and N. W. Sharpe, *Organometallics*, 1991, **10**, 1727–1731.
24 C. D. Hall, J. H. R. Tucker, A. Sheridan, S. Y. F. Chu and D. J. Williams, *J. Chem. Soc., Dalton Trans.*, 1992, 3133–3136.
25 C. D. Hall, J. H. R. Tucker, S. Y. F. Chu, A. W. Parkins and S. C. Nyburg, *J. Chem. Soc., Chem. Commun*, 1993, 1505–1507.
26 C. D. Hall and T-K-U. Truong, *J. Organomet. Chem.*, 1996, **519**, 185–194.
27 C. D. Hall, T-K-U. Truong, J. H. R. Tucker and J. W. Steed, *Chem. Commun.*, 1997, 2195–2196.
28 C. D. Hall, T-K-U. Truong and S. C. Nyburg, *J. Organomet. Chem.*, 1997, **547**, 281–286.
29 C. D. Hall and N. Djedovic, *J. Organomet. Chem.*, 2002, **648**, 8–13.
30 F. Fades, J.-P. Desvergne, H. Bouas-Laurent, J. M. Lehn, Y. Barrans, P. Marsau, M. Meyer and A-M. Albrecht-Gary, *J. Org. Chem.*, 1994, **59**, 5264–5271.
31 B. Witulski, Y. Zimmerman, V. Darcos, J-P. Desvergne, D. M. Bassani and H. Bouas-Laurent, *Tetrahedron Lett.*, 1998, **39**, 4807–4808.
32 K. Kubo, R. Ishige and T. Sakurai, *Talanta*, 1999, **49**, 339–344.
33 (*a*) C. D. Hall, N. W. Sharpe, I. P. Danks and Y. P. Sang, *J. Chem. Soc., Chem. Commun.*, 1989, 419–421; (*b*) P. D. Beer, A. D. Keefe, H. Sikanyika and C. Blackburn J. F. McAleer, *J. Chem. Soc., Dalton Trans.*, 1990, 3289–3294; (*c*) M. C. Grossel, D. G. Hamilton, J. I. Fuller and E. Millan-Barios, *J. Chem. Soc., Dalton Trans.*, 1997, 3471–3477.
34 P. D. Beer, *Chem. Soc. Rev.*, 1989, **18**, 409–450.
35 H. Plenio and R. Diodone, *Inorg. Chem.*, 1995, **34**, 3964–3972.
36 L. T. Mimms, G. Zampighi, Y. Nozaki, C. Tanford and J. A. Reynolds, *Biochemistry*, 1981, **20**, 833–840.
37 D. C. Buster, J. F. Hinton, F. S. Millett and D. C. Shungu, *Biophys. J.*, 1988, **53**, 145–152.
38 J. Sandstrom, *Dynamic NMR Spectroscopy*, Academic Press, London, 1982.
39 A. J. Williams, in *Microelectrode Techniques – The Plymouth Workshop Handbook*, 2nd ed., D. Ogden (Ed); The Company of Biologists Ltd., Cambridge, 1994, p 79–101.